Supplement of

The effect of organic nucleation on the indirect radiative forcing with a semi-explicit chemical mechanism for highly oxygenated organic molecules (HOMs)

Xinyue Shao[1,2], Minghuai Wang[1,2], Xinyi Dong[1,2], Yaman Liu[1,4], Stephen R. Arnold[5], Leighton A. Regayre[5,6,7], Duseong S. Jo[8], Wenxiang Shen[1,2], Hao Wang[1,2], Yue Man[1,4], Jingyi Wang[1,2], Wenxin Zhang[1,2], and Ken S. Carslaw[5]

[1]School of Atmospheric Science, Nanjing University, Nanjing, 210023, China
[2]Joint International Research Laboratory of Atmospheric and Earth System Sciences & Institute for Climate and Global Change Research, Nanjing University, Nanjing, 210023, China
[3]Frontiers Science Center for Critical Earth Material Cycling, Nanjing University, Nanjing, China
[4]Zhejiang Institute of Meteorological Sciences, Hangzhou, 310008, China
[5]School of Earth and Environment, University of Leeds, Leeds, LS2 9JT, UK
[6]Met Office Hadley Centre, Exeter, Fitzroy Road, Exeter, Devon, EX1 3PB, UK
[7]Centre for Environmental Modelling and Computation, School of Earth and Environment, University of Leeds, Leeds, LS2 9JT, UK
[8]Atmospheric Chemistry Observations and Modeling Laboratory, National Center for Atmospheric Research, Boulder, CO 80103, USA

Correspondence to: Minghuai Wang (minghuai.wang@nju.edu.cn), Xinyi Dong (dongxy@nju.edu.cn)

Text S1. Description of the Newly Added Chemical Mechanisms

Figure S1 shows a flowchart of the HOMs mechanism implemented into CAM6-Chem and Table S1 shows the main chemical reactions added into CAM6-Chem. In general, monoterpenes (including α-pinene, β-pinene, limonene and myrcene) are oxidized by OH radicals or O_3 to form MT-aRO_2 and MT-bRO_2 radicals (reactions 1-2 listed in Table S1, with only reactions involving α-pinene shown as an example). MT-bRO_2 undergo multi-step autoxidation reactions to form HOMs with 10 carbon atoms (C10-HOMs) (green arrows in Fig. S1 and reactions 3-4 in Table S1). The intermediates for the autoxidation are MT-cRO_2 and MT-HOM-RO_2. The MT-HOM-RO_2 radical represents the RO_2 radicals that undergo two or multi-step autoxidation. On the one hand, MT-HOM-RO_2 radicals are further oxidized to form C10-HOMs (reaction 8-10 in Table S1). On the other hand, all the MT-RO_2 radicals (including MT-aRO_2, MT-bRO_2, MT-cRO_2, and MT-HOM-RO_2) undergo self- and cross-reactions (orange arrows in Fig. S1) to form accretion products (C15 and C20) (reactions 5-7 in Table S1, with only reactions involving MT-aRO_2 shown as an example). The formation processes of C10-HOMs can be terminated by several oxidants (gray arrows in Fig. S1). SOA is formed via gas-particle partitioning processes of C10-HOMs, C15 and C20 (blue dashed arrows in Fig. S1).

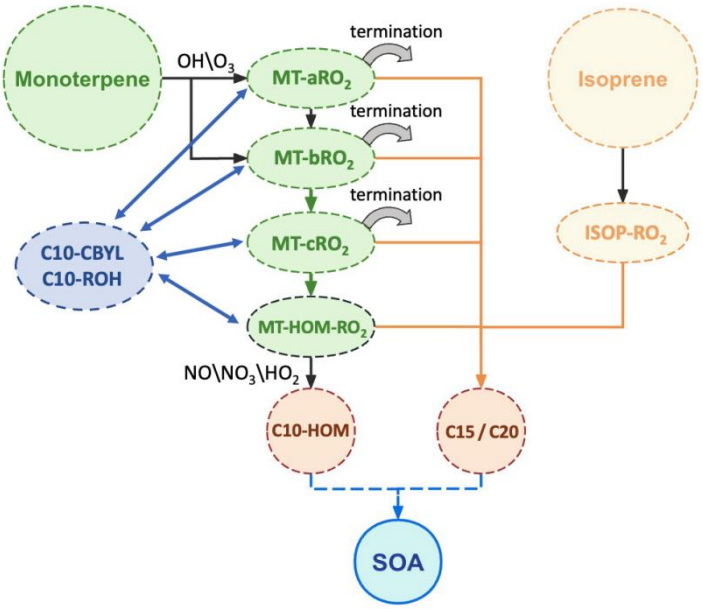

Figure S1. The flow chart of the formation and gas-particle partitioning processes of HOMs and accretion products. The green arrows represent the autoxidation reactions. The gray curved solid arrows represent the termination reactions. The yellow arrows represent the self- and cross-reactions. The blue arrows represent the conversion between C10-CBYL\C10-ROH and MT-RO2 radicals. The blue dashed arrows represent the gas-particle partitioning processes.

Table S1. Main chemical reactions added in CAM6-Chem

Index	Reactions
1	APIN + OH → 0.25*$APINO_2$ + 0.75*MT-bRO_2
2	APIN + O_3 → 0.736*$APINO_2$ + 0.064*MT-bRO_2 + 0.77*OH + 0.066*$TERPA2O_2$ + 0.22*H_2O_2 + 0.044*TERPA + 0.002*TERPACID + 0.034*TERPA2 + 0.17*HO_2 + 0.17*CO + 0.27*CH_2O + 0.054*$TERPA2CO_3$
3	MT-bRO_2 → MT-cRO_2
4	MT-cRO_2 → MT-HOM-RO_2
5	MT-aRO_2 + MT-aRO_2 → 0.893*C_{10}-CBYL + 0.29*C_{10}-ROH + 0.603*HO_2 + 1.34*HYDRALD + 0.067*MT-bRO_2 + 0.04*SOAGac20
6	MT-aRO_2 + MT-bRO_2 → 0.96*C_{10}-CBYL + 0.29*C_{10}-ROH + 0.67*HO_2 + 1.34*HYDRALD + 0.04*SOAGac20
7	MT-aRO_2 + ISOP-RO_2 → 0.4465*C_{10}-CBYL + 0.145*C_{10}-ROH + 0.145*ROH + 0.603*HO_2 + 1.485*HYDRALD + 0.0335*MT-bRO_2 + 0.04*SOAGac15
8	MT-HOM-RO_2 + HO_2 → SOAGhma + O_2
9	MT-HOM-RO_2 + NO → 0.8*NO_2 + 0.8*HO_2 + 0.4*SOAGhmb + 0.8*HYDRALD + 0.2*SOAGhmn
10	MT-HOM-RO_2 + NO_3 → HO_2 + NO_2 + 0.5*SOAGhmb + HYDRALD

Table S2. Species for HOMs and ACC formation mechanism.

Species	Molecular formula	Description
APIN [b]	$C_{10}H_{16}$	α-pinene
$APINO_2$ [b]	$C_{10}H_{17}O_3$	peroxy radical from OH +α-pinene reaction
$MT\text{-}bRO_2$ [a]	$C_{10}H_{16}O_4$	RO_2 from monoterpene+O_3/OH that can undergo autoxidation
$MT\text{-}cRO_2$ [a]	$C_{10}H_{16}O_6$	RO_2 from $MT\text{-}bRO_2$ autoxidation
$MT\text{-}HOM\text{-}RO_2$ [a]	$C_{10}H_{16}O_8$	RO_2 from $MT\text{-}cRO_2$ autoxidation
SOAGhma [a]	$C_{10}H_{14}O_9$	gas-phase C10 HOMs product without nitrate from HO_2 reaction
SOAGhmb [a]	$C_{10}H_{14}O_9$	gas-phase C10 HOMs product without nitrate from NO and NO_3 reaction
SOAGhmn [a]	$C_{10}H_{14}O_9N$	gas-phase C10 HOMs product with nitrate from NO reaction
SOAGac15 [a]	$C_{15}H_{18}O_7$	gas-phase C15 accretion product from isoprene-derived RO_2 (ISOP-RO_2) + MT-RO_2
SOAGac20 [a]	$C_{20}H_{32}O_8$	gas-phase C20 accretion product from MT-RO_2 + MT-RO_2
ROH [a]	C_3H_8O	lumped alcohols with more than 2 carbons
C_{10}-CBYL [a]	$C_{10}H_{17}O_3$	Carbonyl with 10 carbon atoms
C_{10}-ROH [a]	$C_{10}H_{17}O_3$	Alcohol with 10 carbon atoms
CH_2O [b]	CH_2O	formaldehyde
HO_2 [b]	HO_2	hydroperoxyl radical
H_2O_2 [b]	H_2O_2	hydrogen peroxide
HYDRALD [b]	$HOCH_2CCH_3CHCHO$	lumped unsaturated hydroxycarbonyl
TERPA [b]	$C_{10}H_{16}O_2$	aldehyde terpene product with no double bonds that contains a ring like pinonaldehyde
TERPACID [b]	$C_{10}H_{16}O_4$	carboxylic acid/peracid from TERPA
TERPA2 [b]	$C_9H_{14}O_2$	TERPA oxidation product with no double bonds that contains an aldehydic group
$TERPA2O_2$ [b]	$C_9H_{15}O_4$	TERPA peroxy radical 2nd step
$TERPA2CO_3$ [b]	$C_9H_{13}O_4$	acyl peroxy radical from TERPA2

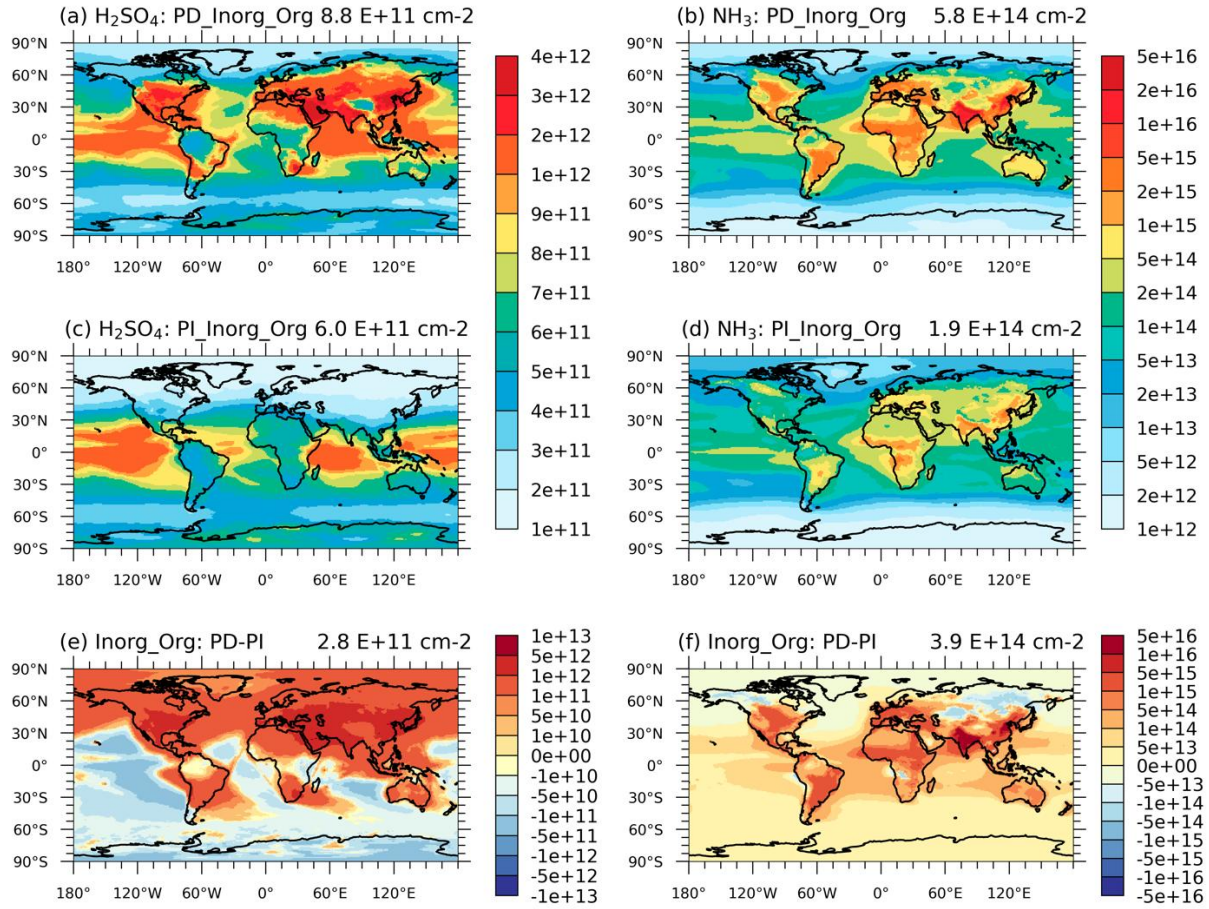

Figure S2. The Spatial distribution of the simulated vertically-integrated H_2SO_4 and NH_3 in PD_Inorg_Org **(a and b)** and PI_Inorg_Org **(c and d)** (unit: cm^{-2}). The differences in these variables between PD and PI environments is shown in **e and f**. Global mean values are shown on the top right of each figure. Model experiments are described in **Table 2** and model data come from monthly mean value over 10 years.

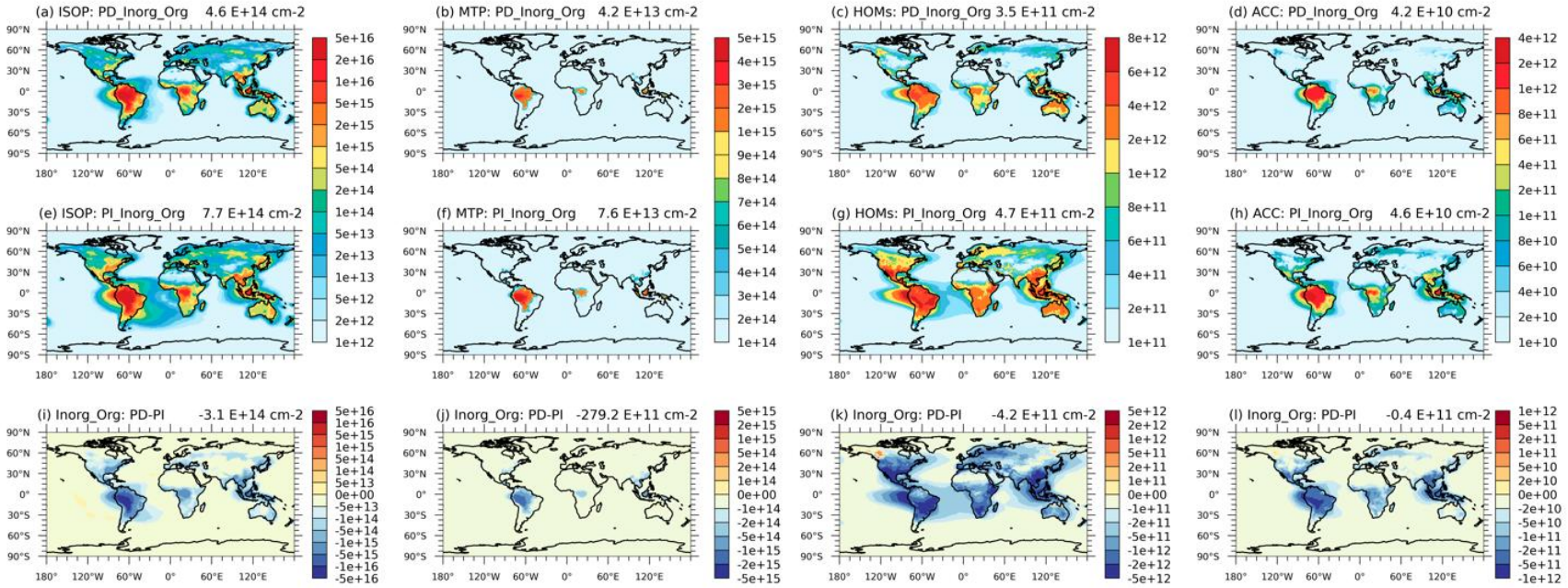

Figure S3. The Spatial distribution of the simulated vertically-integrated isoprene (ISOP) monoterpene (MTP), highly oxygenated organic molecules (HOMs), and accretion products (ACC) in PD_Inorg_Org **(a, b, c, and d)** and PI_Inorg_Org **(e, f, g, and h)** (unit: cm^{-2}). The differences in these variables between PD and PI environments is shown in **i, j, k, and l**. Global mean values are shown on the top right of each figure. Model experiments are described in **Table 2** and model data come from monthly mean value over 10 years.

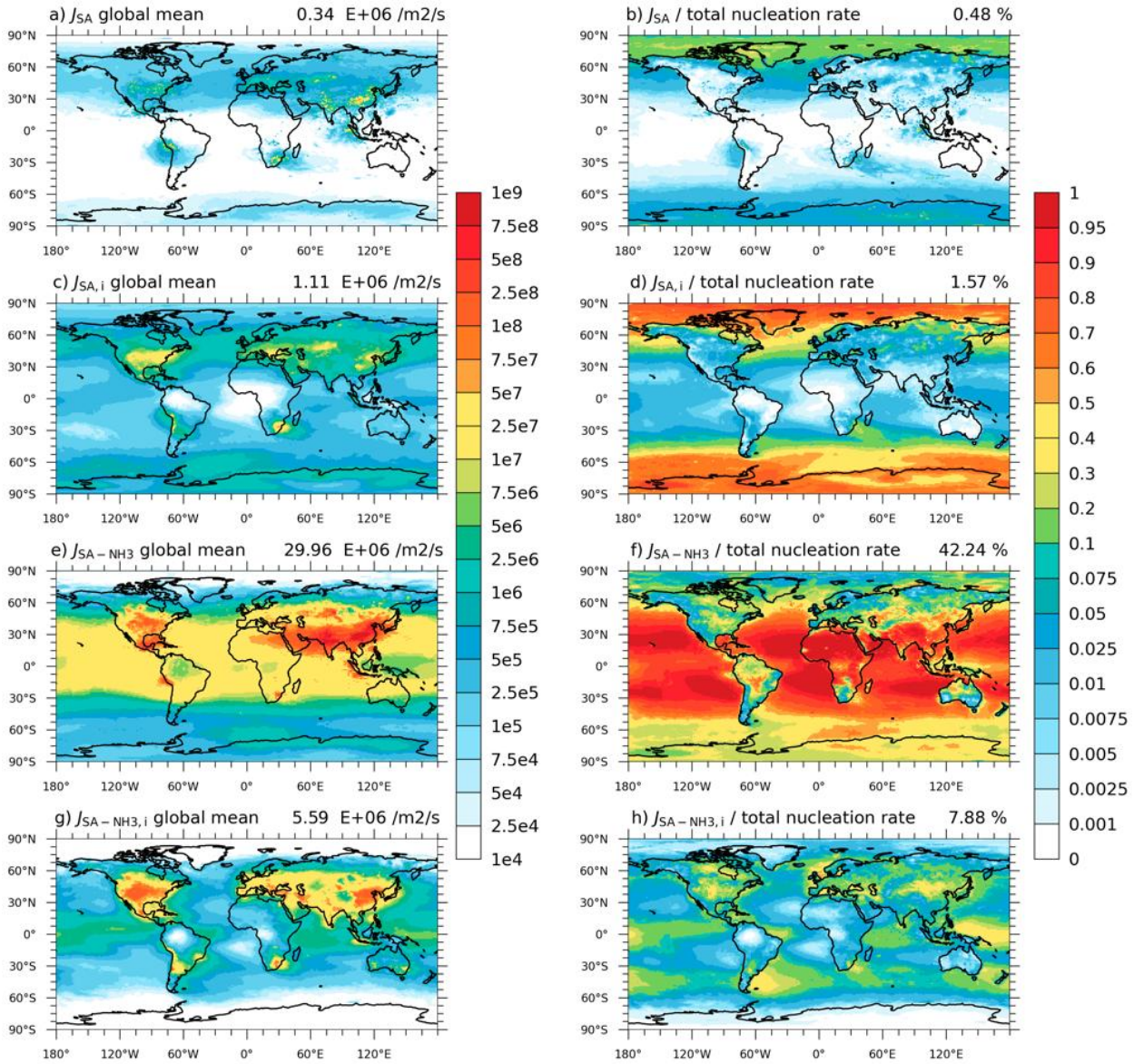

Figure S4. The vertically-integrated inorganic binary neutral nucleation rate **(a)**, binary ion-induced nucleation rate **(c)**, ternary neutral nucleation rate **(e)**, and ternary ion-induced nucleation rate **(g)** within the troposphere (unit: m^{-2} s^{-1}) and their contribution **(b, d, f, and h)** for total nucleation rate in the PD environment of the Inorg_Org case. Global mean values are shown on the top right of each figure. Model experiments are described in **Table 2** and model data come from monthly mean value over 10 years.

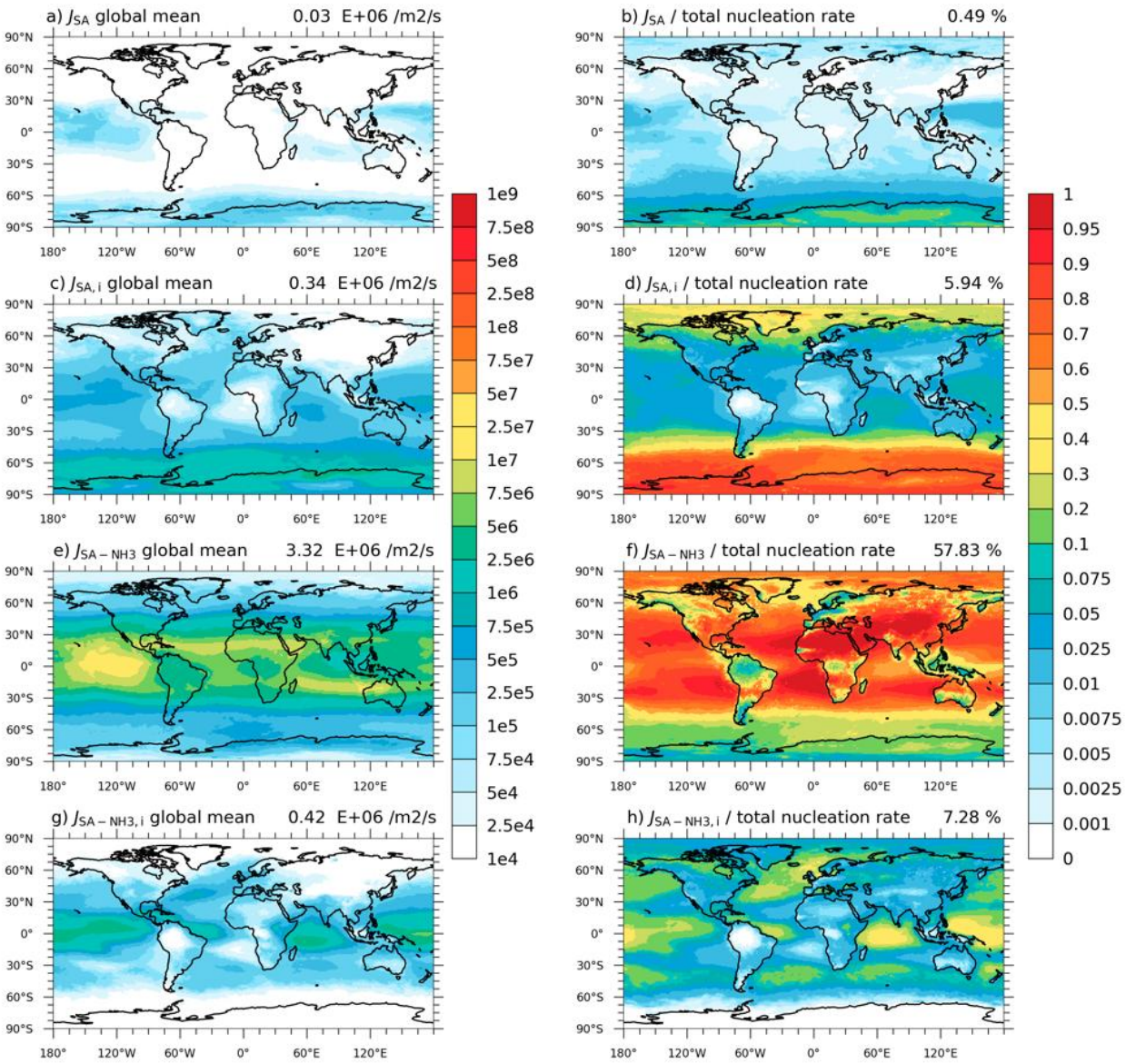

Figure S5. Same as **Figure S4**, but for PI environments.

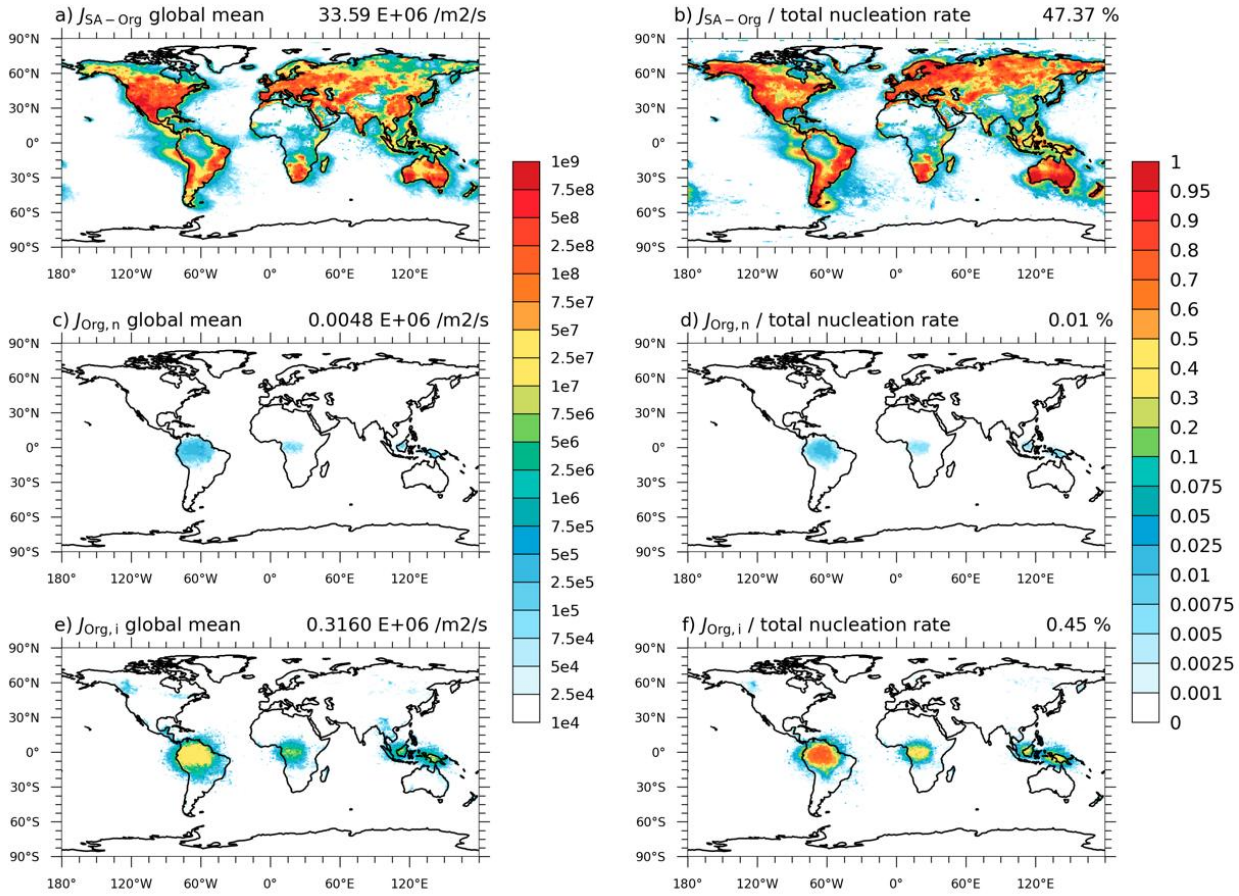

Figure S6. The vertically-integrated heteromolecular nucleation rate of sulfuric acid and organics ($J_{SA\text{-}Org}$) **(a)**, neutral pure organic nucleation rate ($J_{Org,n}$) **(c)**, and ion-induced pure organic nucleation ($J_{Org,i}$) **(e)** within the troposphere (unit: m^{-2} s^{-1}) and their contribution **(b, d, and f)** for total nucleation rate in the PD environment of the Inorg_Org case. Global mean values are shown on the top right of each figure. Model experiments are described in **Table 2** and model data come from monthly mean value over 10 years.

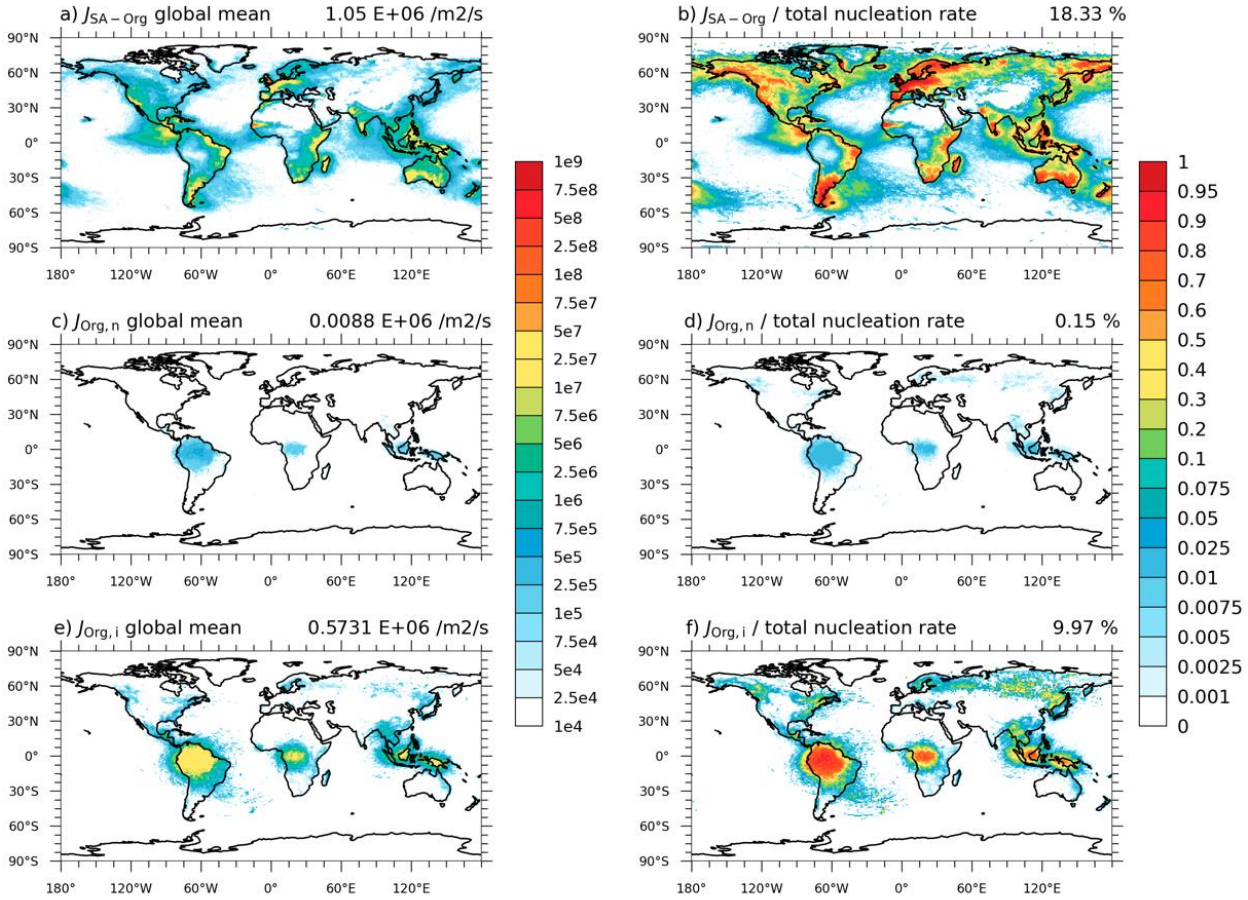

Figure S7. Same as **Figure S6**, but for PI environments.

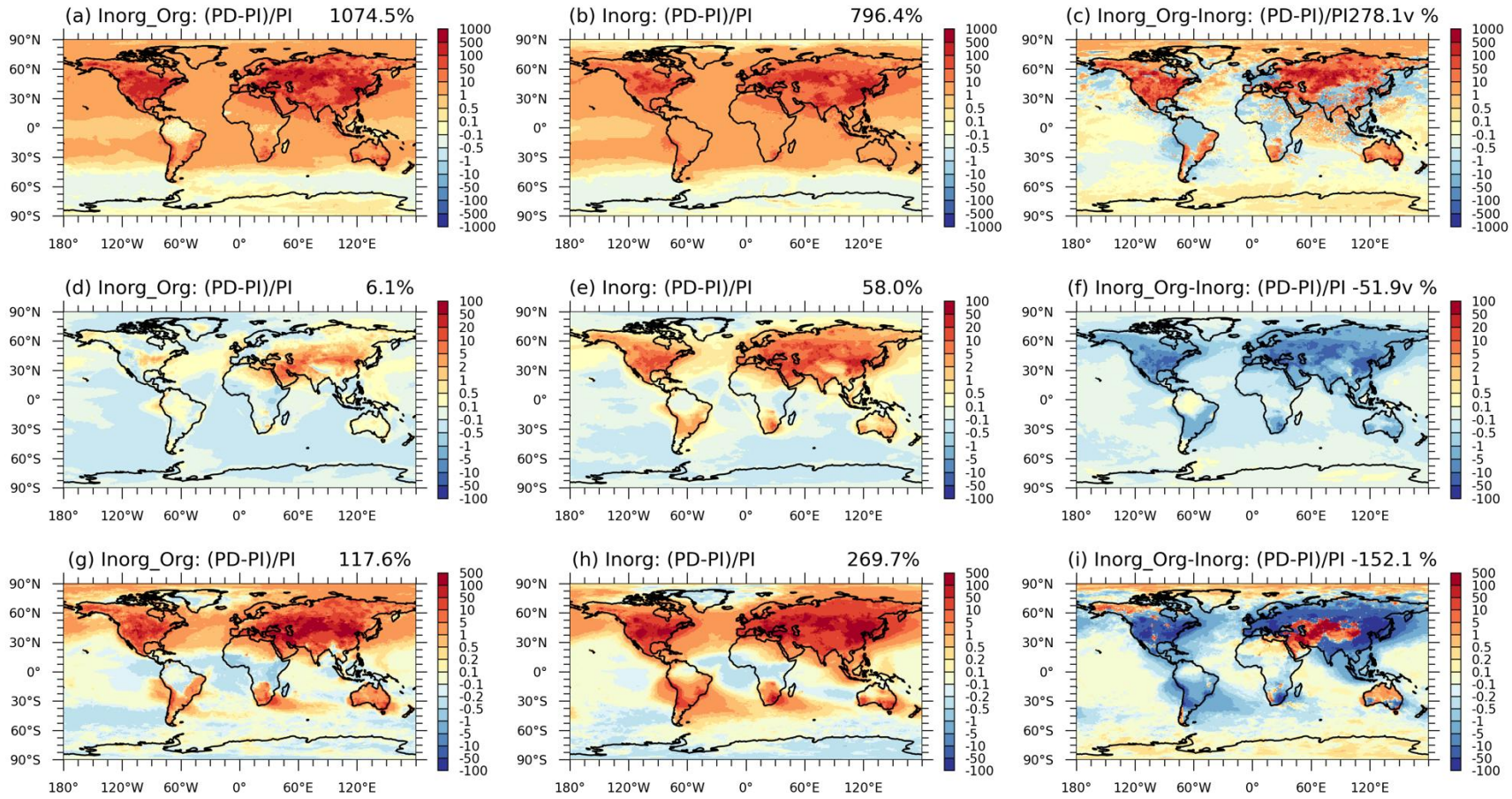

Figure S8. The relative change (unitless) of vertically-integrated nucleation rate ($j_{1.7nm}$), vertically-mean sub-20nm growth rate, and vertically-integrated apparent nucleation rate (j_{20nm}) in PD experiments compared to PI environments (i.e., (PD-PI)/PI) in Inorg_Org **(a, d, and g)** and Inorg **(b, e, and h)**. The difference in these variables between with and without organic NPF is shown in **c, f, and i**.

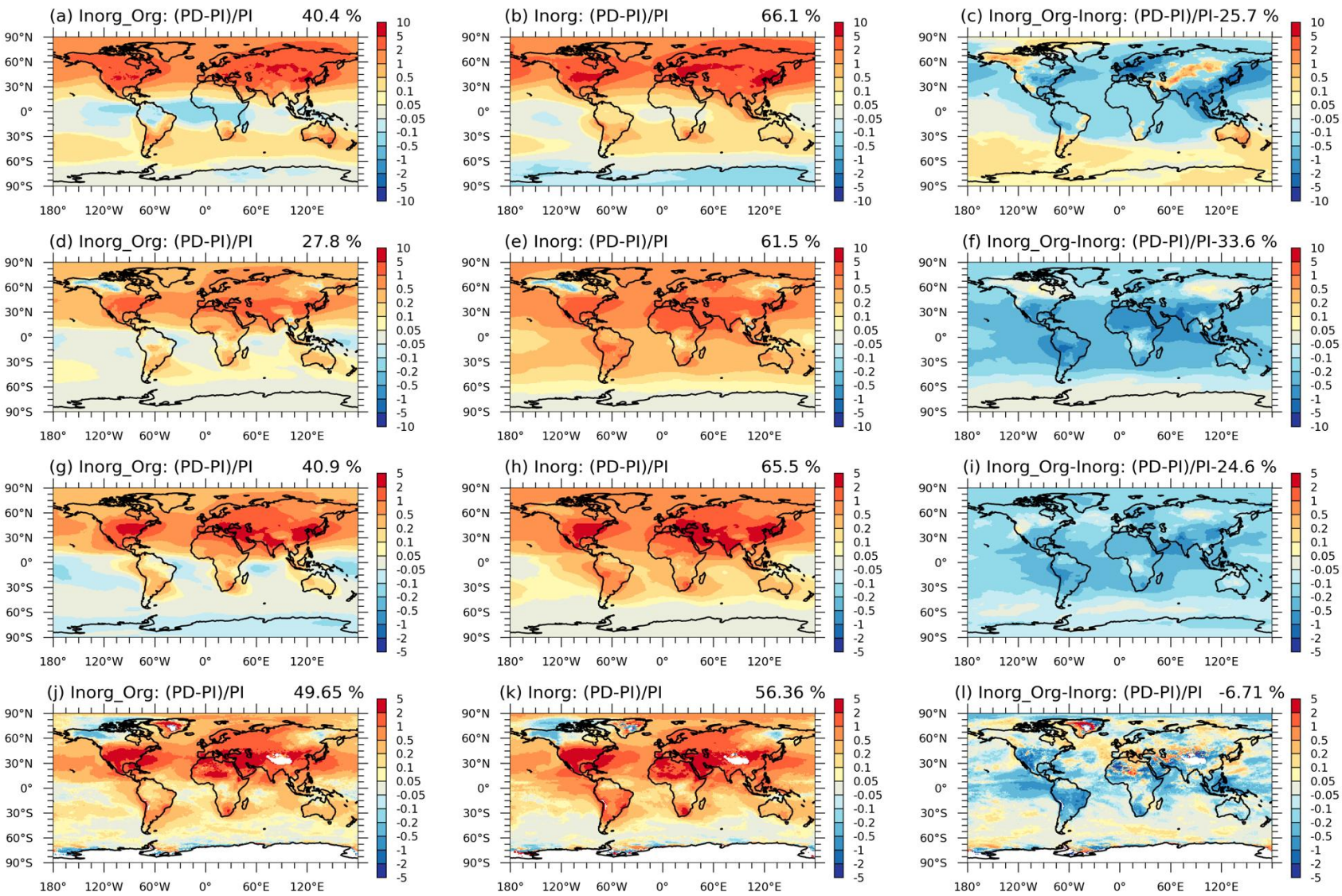

Figure S9. The relative change (unitless) of vertically-integrated aerosol number in Aitken mode, vertically-integrated aerosol number in accumulation mode, vertically-integrated CCN number at 0.2% supersaturation (ss) and cloud droplet number concentration (CDNC) at the top of low clouds in PD experiments compared to PI environments (i.e., (PD-PI)/PI) in Inorg_Org **(a, d, g, and j)** and Inorg **(b, e, h, and k)**. The difference in these variables between with and without organic NPF is shown in **c, f, i, and l**.

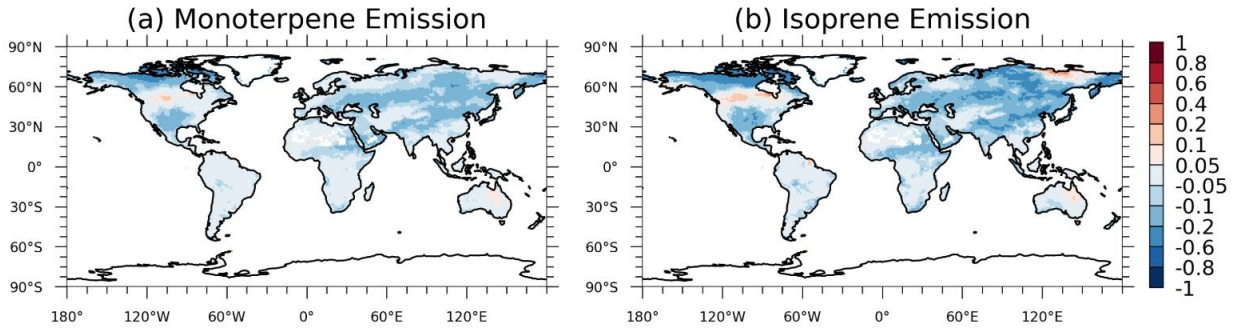

Figure S10. Spatial distribution of the relative difference of monoterpene **(a)** and isoprene **(b)** emission in PD_Inorg_Org and PI_Inorg_Org (unitless). Global mean values are shown on the top right of each figure.

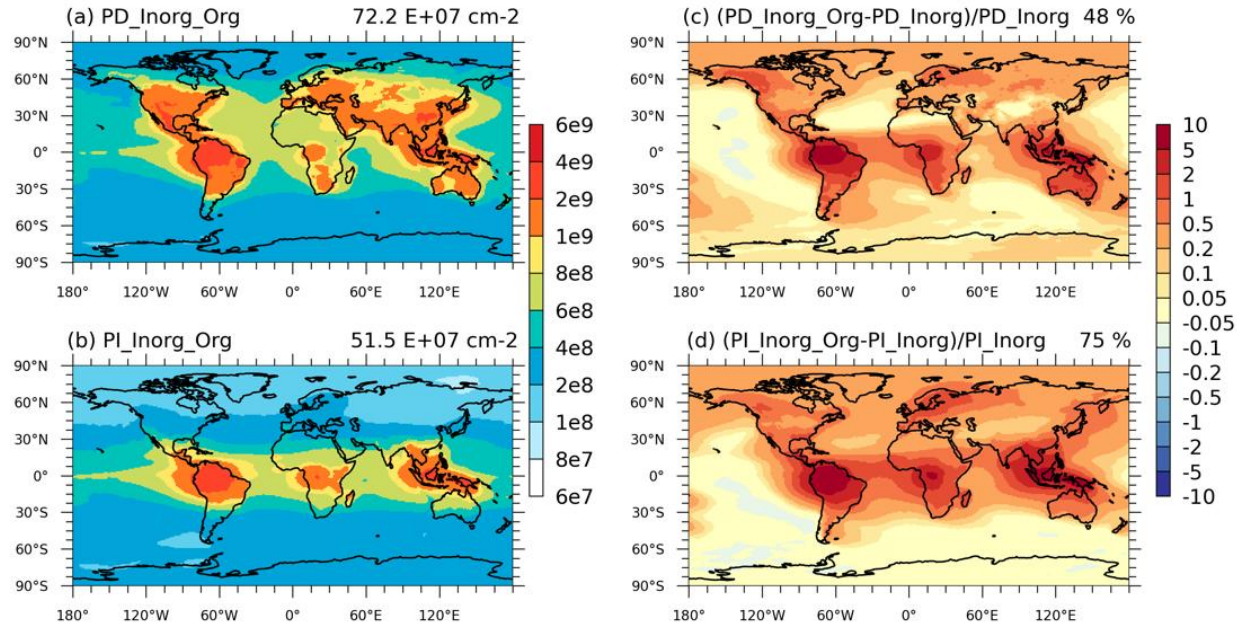

Figure S11. Spatial distribution of the simulated vertically-integrated aerosol number concentration in Aitken mode in **(a)** PD_Inorg_Org and **(b)** PI_Inorg_Org (unit: cm^{-2}). The relative change after adding organic NPF is shown in PD and PI environments are shown in **(c)** and **(d)**. Global mean values are shown on the top right of each figure.

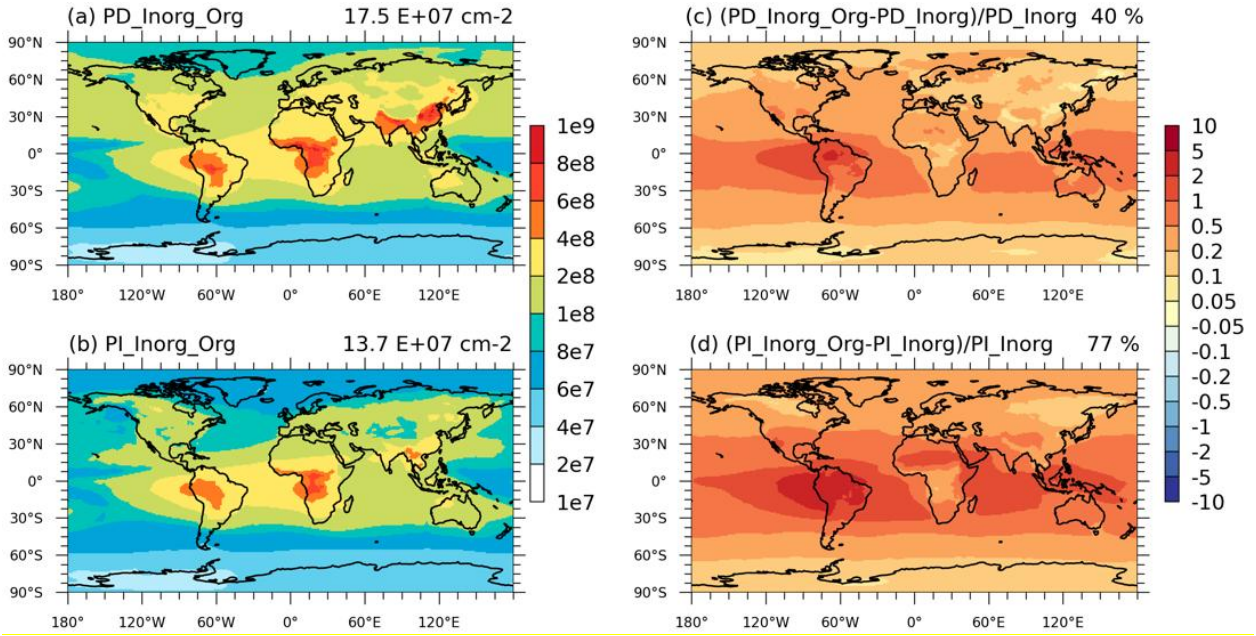

Figure S12. Spatial distribution of the simulated vertically-integrated aerosol number concentration in accumulation mode in **(a)** PD_Inorg_Org and (b) PI_Inorg_Org (unit: cm^{-2}). The relative change after adding organic NPF is shown in PD and PI environments are shown in **(c)** and **(d)**. Global mean values are shown on the top right of each figure.

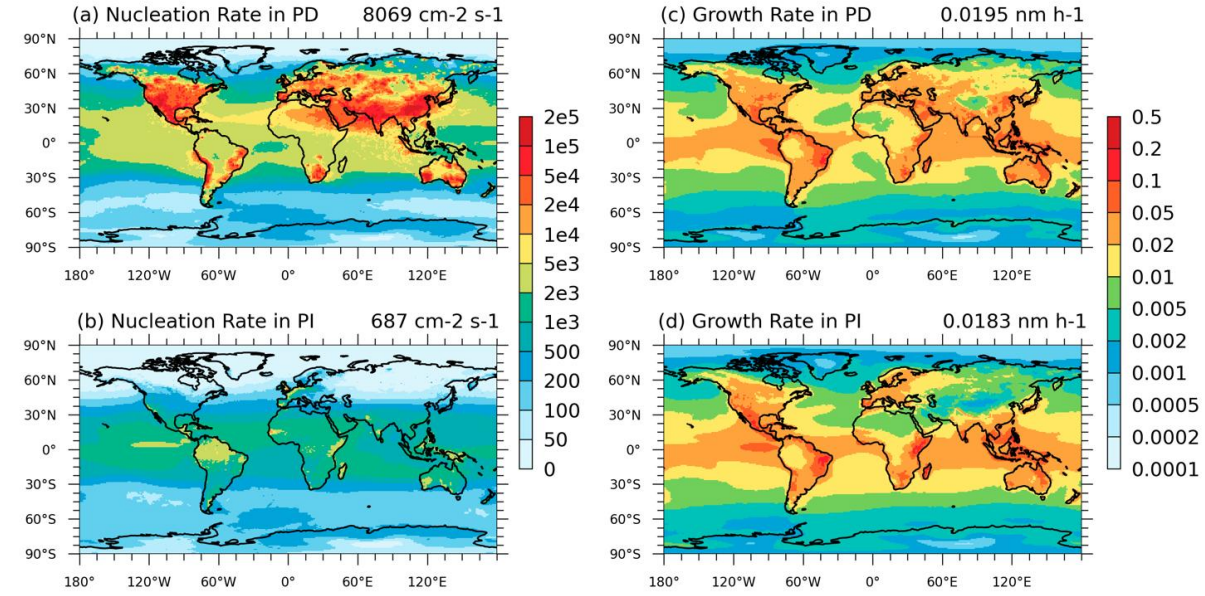

Figure S13. Spatial distribution of the simulated vertically-integrated nucleation rate ($j_{1.7nm}$) in **(a)** PD_Inorg_Org and **(b)** PI_Inorg_Org (unit: $cm^{-2}\ s^{-1}$). Spatial distribution of the simulated vertically-mean growth rate in PD_Inorg_Org **(c)** and **(d)**. Global mean values are shown on the top right of each figure.

Table S3. Main aerosol budget in Aitken and accumulation mode of CAM6-Chem

	Aitken Mode				Accumulation Mode			
	PD		PI		PD		PI	
	Inorg	Inorg_Org	Inorg	Inorg_Org	Inorg	Inorg_Org	Inorg	Inorg_Org
Nucleation (cm^{-2} s^{-1})	1805	4411	359	1805	/	/	/	/
Dry deposition (m^{-2} s^{-1})	162	651	32	125	72	82	40	46
Wet Deposition (m^{-2} s^{-1})	253	765	80	432	100	131	50	82
Coagulation (m^{-2} s^{-1})[a]	1050	2853	227	1157	56	74	26	44
Condensation (m^{-2} s^{-1})[b]	116	182	51	109	116	182	51	109

[a] Coagulation represents aerosol coagulation sink within each mode, excluding inter-modal coagulation.
[b] Condensation represents the rate of aerosol growth from Aitken to accumulation mode though gas (including sulfuric acid and volatile organic compounds) condensation.